Evidences of instantaneous dynamic triggering during the seismic sequence of year 2000 in South Iceland.

A. Antonioli[1], M.E. Belardinelli[2], A. Bizzarri[3], K.S. Vogfjord[4]

[1]Istituto Nazionale di Geofisica e Vulcanologia, Via di Vigna Murata 605, 00143 Rome, Italy, antonioli@ingv.it, now at University of Ulster, Geophysics Research Group, School of Environmental Science, Coleraine, Co. Derry, BT52 1SA, N. Ireland.

[2]Settore di Geofisica, Dipartimento di Fisica, Universita' di Bologna, Viale Berti-Pichat 8, 40127 Bologna, Italy, elina@ibogfs.df.unibo.it.

[3]Istituto Nazionale di Geofisica e Vulcanologia, Sede di Bologna, Sezione di Sismologia e Tettonofisica, Via Donato Creti 12, 40128 Bologna, Italy, bizzarri@bo.ingv.it

[4]Icelandic Meteorological Office, Physics Department, Bustadavegur 9, 150 Reykjavik, Iceland, vogfjord@vedur.is

Abstract

We analyze the coseismic stress perturbation during the June 17th, 2000 South Iceland seismic sequence; the mainshock (Ms 6.6) was followed by three large events within few tens of seconds (8, 26, and 30 s, respectively) located within 80 km. The aim of this paper is to investigate short-term fault interaction and instantaneous triggering. This happens when a fault perturbed by a stress change fails

before the end of the transient stress perturbation. We compute the shear, normal, and Coulomb stress changes as functions of time in a stratified elastic half-space by using discrete wavenumber and reflectivity methods. We calculate dynamic stresses caused by the mainshock at the hypocenters of these three subsequent events. Our numerical results show that the onset of the last two events is slightly delayed with respect to the arrival time of the second positive peak of Coulomb stress variation, while the first event occurred after the first positive stress peak. We have also analysed the response of a spring-slider system representing a fault governed by a rate- and state-dependent friction law, perturbed by shear and normal stress variations caused by the mainshock. The fault response to the computed stress perturbations is always clock advanced. We have found suitable constitutive parameters of the modelled fault that allow the instantaneous dynamic triggering of these three earthquakes. If the initial sliding velocity is comparable with the tectonic loading velocity, we obtained failure times close to the observed origin times for low values of the initial effective normal stress.

1. Introduction

The basic assumption of fault interaction studies is that the stress perturbation produced by an earthquake affects the seismogenic potential of other faults (the "perturbed" faults) and the distribution of subsequent seismicity. Dynamic stress changes caused by earthquakes consist of a permanent or static contribution, and a time varying transient contribution. In intermediate to far field conditions the transient component of coseismic stress changes is less attenuated with respect to the permanent one (Cotton and Coutant, 1997, Antonioli et al., 2004). Dynamic stress changes have been modelled to explain complex ruptures with multiple events (Harris and Day, 1993; Belardinelli et al., 1999; Voisin et al., 2000; Antonioli et al., 2003), as well as the distribution of seismicity following an earthquake (e.g. Kilb et al., 2000, Voisin et al., 2004).

This paper aims to provide further evidence to instantaneous dynamic triggering, by investigating the

causative link between a magnitude 6.6 earthquake of year 2000 in South Iceland and three subsequent events observed in intermediate to far field conditions, within the first minute after the first event. Instantaneous triggering occurs if a seismic event follows closely the arrival of seismic waves at its location, and it occurs within the time interval during which the transient seismic signal is above the background noise level in that location. If instantaneous triggering occurs, then the transient part of coseismic stress changes plays a fundamental role. Therefore instantaneous triggering represents a particular case of fault interaction that can't be investigated through a simple analysis of static stress changes, but requires modelling of the complete dynamic stress perturbation caused by an earthquake on neighbouring faults. Additionally, analysis of the temporal response of the perturbed fault is also necessary in order to verify if instantaneous dynamic triggering occurs. The triggering delay is the time required for the perturbed fault to undergo failure, starting from the beginning of the stress perturbation applied to the fault. In order to estimate the triggering delay it is necessary to model the nucleation phase of the perturbed fault by assuming a fault rheology. If instantaneous dynamic triggering occurs, then the triggering delay is of the order of the duration of the transient part of the dynamic stress perturbations applied to the fault. Effects of fault interaction characterized by larger triggering delays will be referred simply as "delayed" and in these particular cases we do not consider the triggering to be instantaneous.

Recent studies investigated the relative importance of transient stress changes with respect to permanent stress changes in fault interactions. According to Voisin et al. (2004) the effects of the two stress perturbations are indistinguishable in particular they both can provide delayed effects if slip-weakening friction law is assumed as a rheology for perturbed faults. A similar conclusion was proposed by Parson (2005), by using a modified version of the rate- and state-dependent friction laws for the perturbed faults. The latter might take into account the alteration of frictional contacts in the neighbouring faults caused by dynamic shaking. According to other studies (e.g. Ziv, 2003) dynamic

stress changes are not necessary to explain delayed triggering and, even in far field conditions, delayed effects can be explained in terms of multiple interactions caused by permanent stress changes due to previous aftershocks, each of which acts as a mainshock and produces aftershocks (see also Felzer et al., 2002).

Some observations (e.g. Brodsky et al., 2000, Antonioli et al., 2003, Eberhart-Phillips et al., 2003, Tibi at al., 2003, Gomberg et al., 2004, Brodsky and Prejan, 2005) provide support to instantaneous dynamic triggering mainly in intermediate to far field conditions. Observations supporting instantaneous dynamic triggering are not very numerous since detection of events before the end of shaking caused by a triggering earthquake is difficult, especially in near field conditions. Delayed effects are much more numerous than instantaneous triggering effects therefore those considered in this study have to be regarded as an exceptional data set.

Nucleation studies assuming a rate- and state- dependent rheology suggest that instantaneous triggering is the most likely interaction effect due to purely transient stress changes (Gomberg et al., 1998, Belardinelli et al., 2003). However these studies suggest that generally large amplitudes of transient stress changes compared to the direct effect of friction are necessary to provide instantaneous dynamic triggering. This can be a disadvantage in the framework of fault interaction, where coseismic stress changes are generally at least one order of magnitude lower than the stress drop of the perturbing mainshock, especially in intermediate and far field conditions. This problem is not present in nucleation studies assuming a slip-dependent rheology, where triggering delays are typically smaller than few tens of seconds (e.g. Voisin et al., 2000, Monelli, 2004). Therefore, in order to explain instantaneous triggering, assuming a slip-weakening constitutive equation is certainly suitable, but it does not add new contributions to fault interaction studies, unlike facing the problem with rate- and state-dependent friction laws. The latter is widely adopted fault rheology in the framework of fault interaction studies, since it can provide a large range of triggering delays associated with permanent stress changes. In

particular, rate- and state-dependent friction was assumed in nucleation studies aiming to explain the temporal distribution of aftershock sequences, or Omori law (e.g. Gomberg et al., 2005 for references). For these reasons, this paper aims to further investigate the conditions allowing instantaneous triggering under the assumption of a rate- and state-dependent friction for the perturbed faults.

In the sequence of year 2000 in the South Iceland Seismic Zone (SISZ) three events were detected in the first minute after the June17 earthquake (Vogfjord, 2003) within 90 km distance from its epicenter. The origin time of these events correlates with the arrival time of seismic waves generated by the June17 mainshock, as they swept westward, suggesting a causative link between them and the mainshock. We investigate this possibility in the first part of the paper by analyzing the temporal evolution of dynamic stresses generated by the mainshock at the hypocenters of these three early events. We will show that all the three events occurred before the assessment of the static stress level in their hypocenter location, suggesting instantaneous dynamic triggering. In the second part of the paper we assume a rate- and state-dependent fault rheology and we perform direct modelling of the temporal response of a fault to the stress perturbations computed in the first part of the paper. These simulations were made in order to investigate model constraints for instantaneous triggering to occur in the three observed cases.

2. The June 2000 seismic sequence in South Iceland

The sequence of interest in this paper took place in the South Iceland Seismic Zone and the Reykjanes Peninsula (SISZ and RP in Figure 1) starting on June 17, 2000. The zone is a left lateral EW transform zone that connects the Western Volcanic Zone (WVZ) and the Reykjanes Peninsula (RP) oblique rift zone in the west and the Eastern Volcanic Zone (EVZ) in the east. The SISZ is one of the presently active areas of strike slip faulting in Iceland where large earthquakes have occurred in the recent past. The last major earthquake of the area (and the first being instrumentally recorded) was the

Ms=7.0 shock of 1912 that occurred in the easternmost part of the SISZ, while the largest historical earthquake occurred in 1784 (Ms=7.1) and was followed two days later by another slightly smaller event (Ms=6.7) about 30 km to the west. Moreover, since the nineteenth century, historical records describe sequences of large earthquakes over periods lasting from days to months. The time interval between the sequences ranges between 45 and 112 years (Einarsson et al., 1981). These earthquake sequences occurred in 1630-1633, 1732-1734, 1784, 1896, and 2000. Most of the sequences started in the eastern part of the SISZ and migrated towards the west. From August to September 1896 five Ms=6.0-6.9 earthquakes occurred thorough the SISZ, but several historical earthquakes have also occurred as single events (e.g. the 1912 earthquake).

The 2000 sequence started on June 17, at 14:40:41 UTC, with an event of magnitude Ms=6.6 (Pedersen et al., 2001). The hypocenter location was 63.973°N, 20.367°W and 6.3 km depth. A second large event (Ms=6.6) occurred on June 21, at about 17 km west of the June 17 event, at 63.972°N, 20.711°W and 5.0 km depth (Figure 1).

After the June17 mainshock, three events within few tens of seconds (at 8 s, 26 s and 30 s after the mainshock) occurred up to a distance of 80 km along the SISZ and its prolongation along the RP (Figure 1 and Table 1). Most of the short period stations of the local network within 80 km epicentral distance from the June17 mainshock were saturated. The events occurring 26 s and 30 s after the mainshock in turn saturated stations within 20 km from their own epicenters, and they were not detected teleseismically. For these reasons and the short interevent time separation between the mainshock and the subevents occurring in the first minute, the 8 s event and the 30 s event remained undetected for some time.

The sequence was very well monitored by several local networks: digital seismic stations, strong motion network, volumetric strain meter networks and permanent GPS stations in Iceland. Coseismic deformations were measured by GPS stations and InSAR measurements, which constrain distributed

slip models of the two major events (Pedersen et al., 2003). Arnadottir et al. (2003) studied the interaction between the two mainshock faults, by computing the coseismic static stress change in an elastic homogeneous half-space. Static stress changes were found to correlate well with the observed spatial distribution of aftershocks, mainly in the near field. Jónsson et al. (2003) concluded that, near the two main events, poroelastic rebound dominates the observed postseismic deformations in the first few months of the sequence, but the pore fluid flow does not control aftershock duration, even if off fault aftershocks occur mainly in quadrants of decreased pore pressure.

Among the thousands of recorded seismic events following the June 17 and June 21 mainshocks (Hjaltadottir et al, 2005) two additional M≈5 events occurred within the next five minutes from the June 17 mainshock: one just west of the main event after two minutes, the other after almost five minutes (286 s) at 86 km distance on RP (Vogfjord, 2003). These two events occurred after the passage of seismic waves generated by the mainshock at their own epicenter, as will be clear from the result of the next section. Therefore the 2 and 5 minutes events do not represent cases of instantaneous dynamic triggering. Arnadottir et al. (2003) showed that the 2 minutes event was affected by more than 0.2 MPa of permanent Coulomb Failure Function positive variation caused by the mainshock. Arnadottir et al. (2004) showed that the 26 s event and mostly the 30 s event increased permanently the Coulomb Failure Function by 0.1-0.2 MPa at the hypocenter of the 5 minutes event. Both the seismic sources of the 30 s event and the 5 minutes event are affected by uncertainties related to different parameters provided by seismic and geodetic data (Arnadottir et al., 2004, Hjaltadottir et al., 2005, Vogfjord et al.,

2005). These uncertainties can affect significantly direct modelling of the 5 minutes event, mainly if it is considered as a secondary aftershock of the 30 s event, as geodetic data suggest. Nevertheless in the discussion section we will deserve attention to event after 5 minutes in order to check the consistency of our results for the 26 s and 30 s events with the delayed triggering of the 5 minutes event. However in the following section of this paper we will focus our attention mainly on the three

events, which occurred in the first minute after the June 17 mainshock.

3. Dynamic stress interaction

The three events occurred in the first minute after the June17 earthquakes in the SISZ and RP represent potential evidence of instantaneous dynamic triggering; moreover the two RP events occurred in the far field of the June17 mainshock where the static stress values are negligible. To investigate the causative link between these three events and the mainshock, it is necessary to evaluate the dynamic stress changes caused by the mainshock.

We compute the stress field variations as a function of time, $\sigma_{ij}(t)$, due to the June17 mainshock, using the discrete wavenumber and reflectivity code developed by Cotton and Coutant (1997). The Coulomb Failure Function variation is computed according to the following expression

$$\Delta CFF(t) = \Delta\tau(t) + \mu_a \Delta\sigma(t) \qquad (1)$$

where $\Delta\tau(t)$ and $\Delta\sigma(t)$ are the shear stress change and the normal stress change projected on the fault plane of interest, respectively. Normal stresses are assumed as positive for compression and all times are evaluated so that the mainshock origin time is t=0 . The apparent friction coefficient is expressed as $\mu_a=(1-\beta)\mu$, where μ is the friction coefficient and β is the Skempton coefficient, assumed to be equal to 0.4 (Harris, 1998, among many others**)**. In agreement with gross features of mapped surface and subsurface faults of the area (e.g. Belardinelli et al., 2000; Clifton et al., 2003; Clifton and Einarsson, 2005; Hjaltadottir et al., 2005), for all the three possibly triggered events, we project the stress on to right lateral N-S vertical fault planes. Apart from stress conjugate ENE left-lateral structures, also NNE right lateral structures are observed, we verified that small differences in strike (between 0° and 25°) and dip (between 65° and 90°) orientations with respect to north-striking, right lateral and vertical fault planes do not significantly affect the computed *CFF* changes (especially when compared with the more

important medium stratification effects), except for the 8s aftershock, as will be discussed in the next section.

The vertical structural variations of the SISZ region can be reproduced by our layered model. Neglecting this layering may affect the amplitude of dynamic peaks at a given depth and the absolute arrival times of seismic waves at a given location (Antonioli et al., 2004). Our model, however, cannot take into account lateral variations of the crustal structure. We assumed a four layer structure (Figure 2) inferred from travel time studies (Vogfjord et al., 2002) for the East of Hengill region ('He' in Figure 1), where the June 17 mainshock and the 8 s event are located. The assumed structure is a good approximation also to the West of Hengill region, at least down to 8 km depth (Figure 2). Moreover, even if the 26 s and 30 s events occurred west of Hengill, the largest part of the wave path from the mainshock to the aftershocks in the RP (26 s and 30 s events) is in the East of Hengill region.

For the main event (June 17), we assume a bilateral rupture in a Haskell source model with rise times in the range 1-2 s and 2.5 km/s rupture velocity, without focusing on the complexity of the real rupture dynamics, recalling that the use of a more complex rupture history does not play a major role in the dynamic stress redistribution. Antonioli et al. (2004) showed that the only effect of different rupture models is to change slightly the amplitude of local minima and maxima and the frequency content of the stress as a function of time, particularly at the distances between the mainshock and the triggered events. We assume the slip distribution on the fault plane retrieved by a joint inversion of GPS and InSAR data and shown in Arnadottir et al. (2003). The fault parameters for the mainshock lay within a narrow range of estimated values; we adopted a strike angle of 7°, a dip of 86° and a rake of 180° (right lateral strike slip mechanism), on the basis of the aftershocks distribution (Stefansson et al., 2003).

In order to give a general overview of the dynamic stress redistribution in the two aftershock regions, we computed horizontal maps of the time evolution of the ΔCFF on the RP. Snapshots at four different times are shown in Figure 3, at the 26 s aftershock hypocentral depth (8.9 km) adopting a rise time of 1

second. The arrival times of positive peaks of stress waves are slightly advanced with respect to the aftershock origin times. In Figure 3, at 22 seconds, the region of the first event is going to be reached by a positive peak of ΔCFF coming from east. At 26 s (origin time of the second early event), the peak is leaving the aftershock location. Similar results were obtained for the 30 s event, as a consequence the origin time of the two aftershocks correlates with a much lower ΔCFF than the peak value.

In Figures 4 and 5, we show the variations of *CFF*, normal stress and shear stress (ΔCFF(t), $\Delta\sigma$(t), and $\Delta\tau$(t), respectively) as a function of time in the location of the hypocenter of the subsequent events (see Table 1). The values of ΔCFF, $\Delta\sigma$, and $\Delta\tau$ at the origin time of the three aftershocks are denoted by symbols on the dynamic stress curves.

In Figure 4 we show the stress time evolution on the first event that occurred about 8 s after the mainshock (see Figure 1). For the 8 s event, the normal stress counteracts the effect of the shear stress that is supposed to promote the failure. As a result, the ΔCFF dynamic peaks are lower than corresponding peaks in $\Delta\tau$. The timing of the rupture is delayed about two seconds with respect to the first peak of ΔCFF at $t=t^{I}$. At the hypocenter of the other two events (Figure 5), the normal stress change is negligible with respect to the shear one and ΔCFF as a function of time is closer to $\Delta\tau$ in Figure 5 than in Figure 4. Moreover the static values, reached after about 50 s, are much smaller than dynamic peaks, as expected, since the static stress amplitudes decay with distance from the mainshock faster than dynamic stress amplitudes. It is clear from panels a) and b) of Figure 5 that both aftershocks did not occur immediately at the first arrival time of the seismic waves generated by the main event, but they followed closely (about two seconds) the second peak of ΔCFF at $t= t^{II}$, whose amplitude is more than twice the first positive peak. These results could eventually support the idea of instantaneous triggering as a possible explanation of the aftershocks on the RP.

To check the role of the main event's rise time on the dynamic stress amplitudes we computed the

dynamic stress of the main event of June17 for varying rise times between 1 and 2 s. The obtained stress variations as a function of time in the hypocenters of 26 s and 30 s events are similar to those shown in Figure 5, except for being characterized by amplitudes that scale inversely with the rise time. In fact, increasing rise time entails decreasing the slip rate, for a fixed value of slip. Decreasing values of slip rate provides decreasing amplitudes of the load on the fault plane due to previous slip history (Tinti et al., 2004) or, similarly, decreasing synthetic amplitudes of the seismic waves of stress departing from the fault plane. As a result, by increasing the rise time, decreasing stress amplitudes of the synthetic wave of stress can be obtained.

4. The temporal response of a fault to the computed stress change

Observations support the idea of instantaneous dynamic triggering occurring in the three early aftershocks analyzed here. In the previous section we showed that these three events followed closely the arrival of seismic waves at their location, or, at least, they occurred within the time interval during which the dynamic seismic signal was above the background noise level at their location. However the temporal response of a fault subjected to a stress perturbation is controlled by its rheology and this response in principle can be delayed with respect to the stress perturbation application time or it can be negligibly affected by the stress perturbation (e.g. Belardinelli et al., 2003). In this section we perform direct modeling of the temporal response of a fault perturbed by the stress variations computed in the previous section by assuming a rate- and state- dependent friction law. The aim of these simulations is to evaluate model parameters that allow us to obtain a modeled failure time of the perturbed fault that is close to the observed origin time for the three early events, in order to evaluate either the efficiency of the computed stress changes in destabilizing the perturbed faults or the conditions that favor instantaneous dynamic triggering, on the basis of the rheology assumed for these faults.

4.1. System parameters

We made several tests by means of a one-degree of freedom spring-slider analog fault model. In the following we will refer as σ_n^{eff} the effective normal stress acting on a perturbed fault, defined by $\sigma_n^{eff} = \sigma - p_f$ where σ is the component of the stress acting in the host rock and normal to the fault plane and p_f is the pore fluid pressure. We assume a rate- and state-dependent friction τ_f, for an applied time- dependent σ_n^{eff} with $\sigma_n^{eff}(t) = \sigma_0 + \Delta\sigma(t)$; σ_0 is the effective normal stress before the earthquake (or initial effective normal stress) and $\Delta\sigma$(t) normal stress perturbation. Indicating with V and Ψ the sliding velocity and the state variable at a time t, respectively, the frictional resistance τ_f is described by the following set of equations

$$\tau_f(V,\Psi,t) = \left[\mu_* + a\ln\left(\frac{V}{V_*}\right) + b\ln\left(\frac{\Psi V_*}{L}\right)\right]\sigma_n^{eff}$$

$$\dot{\Psi} = 1 - \frac{\Psi V}{L} - \alpha_{DL}\frac{\Psi\dot{\sigma}_n^{eff}}{b\sigma_n^{eff}} \qquad (2)$$

(Linker and Dieterich, 1992), where the superimposed dot indicates time derivative, *a, b, L* and α_{DL} are experimental parameters, V_* and μ_* are reference values of the fault sliding velocity and friction coefficient, respectively. The dynamic equation of the spring-slider motion (e.g. Belardinelli et al., 2003) is

$$m\dot{V} = \tau + \Delta\tau(t) - \tau_f \qquad (3)$$

where m is the mass per unit surface, $\Delta\tau$(t) is the shear traction perturbation and $\tau = k(\delta_0 - \delta)$. Here k is the spring stiffness, δ is the slip and $\delta_0 = V_0 t$ is the loading point displacement, V_0 being the loading point velocity. We consider values of the parameter α_{DL} that controls the sensitivity of friction to

normal stress changes in the experimental range 0.25-0.5 (Dieterich and Linker, 1992). If α_{DL}=0 the evolving equation (second equation of (2)) is equal to the standard ageing law that was experimentally derived for constant normal stress (e.g. Roy and Marone, 1996). Then, when we show results for α_{DL}=0, we apply only the shear traction perturbation $\Delta\tau$(t) (formally: $\alpha_{DL} = 0 \Rightarrow \sigma_n^{eff}(t) = \sigma_0$). The loading point velocity (V_0) in the spring slider model is representative of a tectonic strain rate applied to the model fault and V_* is a reference value of sliding velocity. We assumed $V_0 = V_* = 2$ cm/yr to be consistent with observational evidences of background strain rate in the region of interest.

Belardinelli et al. (2003) defined the failure time as the time instant when the fault sliding velocity exceeds a threshold value of V_L = 0.1 m/s. The chosen V_L value is near to the maximum slip velocity obtained in average in our simulations (see Figure 6). Unlike quasi-static spring-slider models where the sliding velocity can be unbounded, for a spring-slider models taking into account the inertial term (as our does), the definition of a threshold velocity is useful in order to discriminate the aseismic response from the seismic response. Roy and Marone (1996) identified the end of the quasi-static regime using a limiting value of the sliding velocity that is of the order of 1 mm/s, for parameter values used in the present study. If V_L = 1 mm/s would be assumed, our failure times would decrease by about

1.5 s and we would identify triggered failures even for $\sigma_0 < 1$ MPa. These effects are not critical for the conclusions of the present study. Moreover, we emphasize that a limiting velocity of 1 mm/s is perhaps more representative of "slow earthquakes", i.e. events mainly developing aseismic slip which is detectable by geodetic techniques on time scales going from minutes to months (Arnadottir et al., 2004).

The reference values of model parameters are listed in Table 2, unless differently specified. Studies on the temporal distribution of earthquakes in the RP (Clifton et al., 2005 and Clifton, 2005, personal communication) suggest an average recurrence time of the order of tens of years. For the chosen parameters and with varying σ_0 from 2 MPa to 20 MPa, we obtain a recurrence time of seismic

instabilities of the spring-slider system ranging between 10 yr and 140 yr, in agreement with the available observations for the RP and the SISZ.

The initial conditions of the fault, at the time t =0 of the stress perturbation application, are $V_i=V(t=0)=V_0$ and $\Psi(t=0)=L/V_i$: the fault is then assumed to be at steady state at the loading point velocity in most of the simulation that will be shown, unless differently specified. For the chosen initial conditions and parameters values, we evaluate t_u, the first instant of failure in unperturbed conditions (i.e. when $\Delta\tau(t)= \Delta\sigma(t)=0$). The computed t_u values vary from 8 months to 97 years by varying the initial effective normal stress value σ_0 between 2 and 100 MPa. This choice of initial conditions implies that the model fault is strongly "clock-advanced" (we have t_u-$t_p \cong t_u$ where t_u- t_p is the clock advance and t_p is the perturbed failure time, e.g. Figure 2 in Gomberg et al., 1997) in each case of instantaneous triggering ($t_p \cong$ tens of seconds).

4.2. The three early events

We impose on the spring-slider fault system the stress perturbations $\Delta\tau(t)$ and $\Delta\sigma(t)$ that we computed at the three hypocenters and then we evaluate the first time instant of failure t_p in perturbed conditions. In Figure 6, for σ_0 =2.5 MPa, we show the evolution of the perturbed fault in terms of sliding velocity $V(t)$ (Figure 6c) and state variable $\Psi(t)$ (Figure 6d) as functions of time t since the perturbing mainshock. The stress perturbations $\Delta\tau(t)$ and $\Delta\sigma(t)$ are those obtained in the 26 s event hypocenter for a 1.6 s rise time. The total applied shear stress $\tau+\Delta\tau(t)$ and effective normal stress $\sigma_0+\Delta\sigma(t)$ are shown in Figures 6a and 6b, respectively. The computed failure instant t_p=25.5 s correlates with the observed origin time (25.9 ± 0.1 s). From Figure 6, it is evident that the sliding velocity follows the shear stress perturbation $\Delta\tau(t)$, whereas the state variable evolution anti-correlates with the normal stress perturbation $\Delta\sigma(t)$, as expected from equation (2).

In order to favor the instantaneous dynamic triggering effect (Figure 6), following Belardinelli et al. (2003), we expect that $\Delta\tau(t)$ should be comparable to the direct effect of friction that scales with $a\sigma_n^{eff}$. As a first choice, we favor dynamic triggering by decreasing the effective normal stress value before the earthquake, σ_0, leaving other parameters unchanged, since several studies argued about the link between the weakness of a fault and low values of effective normal stress in fault zones (e.g. Rice, 1992, Perfettini et al., 2003). Our results, for the 8 s and 26 s aftershocks, are summarized in Figure 7, where it is evident that we obtain a "short term" response of the fault (indicating instantaneous dynamic triggering) only for small values of the effective normal stress (less than 4 MPa, for V_i =2 cm/yr and $\Psi(t=0)=L/V_i$). With larger values of the effective normal stress we obtain a "long term" or delayed response of the fault, where the failure time t_p is generally well after the end of the time varying part of the stress perturbation. We note that the instantaneous effect disappears generally for $\sigma_0 \leq 1$ MPa since the sliding velocity does not reach the threshold value V_L. According to the notation of Boatwright and Cocco (1996), the fault tends to become "weak" with decreasing σ_0 since the difference $k_c-k=(b-a)\sigma_0/L-k$ also decreases. The long term effect shown in Figure 7 is different from the "null" effect associated by Belardinelli et al. (2003) to purely transient stress changes, particularly in Figure 7 the model fault appears as always clock-advanced. The main reason of this is that the stress perturbations here applied have a non-negligible permanent component (Figures 4 and 5a).

In Figures 7a and 7b we show the dependence on the parameter α_{DL} (eq. 2), which affects the fault response mainly in the long term, depending on the particular stress perturbation history applied (the effect on the 8 s aftershock differs from the 26 s aftershock). We emphasize that generally the results obtained in terms of t_p are dependent on the details of the history of the applied stress perturbations, $\Delta\tau(t)$ and $\Delta\sigma(t)$. In particular, we verified that if the static value of $\Delta\tau(t)$ is applied as a pure step at the beginning of the simulation (case 1), we obtained a significantly different time of failure t_p with respect

to the case in which the detailed stress perturbation history, $\Delta\tau(t)$ and $\Delta\sigma(t)$, is applied (case 2). If, in case 2, parameters are suitable to produce the short term response, then in case 1 for the same parameter values we have the long term response. Moreover, if parameters are suitable to have the long term response in both cases, the failure time in case 1 is different from that in case 2, for the same parameter values.

The short term response obtained in Figure 7 for low values of the initial effective normal stress σ_0 does not provide necessarily a modelled failure time t_p close to the observed origin time of the early events. If this is not true, the short term effect shown in Figure 7 does not support the hypothesis of instantaneous dynamic triggering. In Figure 7a, for example, instantaneous dynamic triggering is shown to occur, for $\sigma_0 \leq 3.5$ MPa, with t_p around 12.5 s, that is near t^{II} , the time instant of the second, larger than the first, peak of ΔCFF (Figure 4). We reproduced the origin time of the 8 s event using initial conditions (V_i =20 m/yr and $\Psi(t=0)=1.2\ L/V_i$ that are closer to failure than previously specified and σ_0=1.5 MPa, for other parameters unchanged. The request of close to failure conditions is not necessary if we assume that the 8 s fault strike is 25°. In this case we obtain a perturbed failure time varying between 6.3 s and 7.9 s with varying σ_0 between 1.5 MPa and 2.5 MPa, with the same parameters used to obtain the results shown in Figure 7a. Assuming for the 8 s fault variable values of strike (between 0° and 25°) and dip (between 65° and 90°) with respect to north-striking, right lateral and vertical fault planes (see section 3) , we verified that a strike equal to 25° and a dip equal to 90 degrees provides the largest value of $\Delta CFF(t^I)$.

For the 26 s event we studied the t_p dependence on σ_0 with varying $\Delta\tau(t)$ and $\Delta\sigma(t)$ within the range of uncertainties of dynamic stress modelling. We applied the stress changes that we obtained with varying the rise time between 1 and 2 s: our results are summarized in Figure 7c. For $\sigma_0 \leq 3.5$ MPa, V_i=2 cm/yr, and $\Psi(t=0)=L/V_i$, we obtained failure times t_p in the range 24.2-26.0 s. We will discuss in

the next subsection the effect of different initial conditions showed in Figure 7c. In the case of the 30 s aftershock, assuming a 1.6 s rise time, we obtained t_p in the range 28.1-29.3 s for $\sigma_0 \leq 3.0$ MPa. Therefore for both the 26 s and 30 s aftershocks we obtain average t_p values that are slightly smaller than the observed origin times. However, owing to the simplifications adopted in our modeling, we believe that our results concerning the 26 s and 30 s aftershocks support the inference of dynamic triggering at low values of effective normal stress before these events.

4.3. Conditions for a short term response

The short term response could be favored without changing σ_0 if it was possible to increase the value of initial effective normal stress at which the transition from the short term to the long term response occurs. We refer to this value as σ_0^{max}. In the Appendix σ_0^{max} is shown to decrease by either decreasing a or increasing the initial sliding velocity V_i or considering perturbed faults that are "closer to failure" (e.g. Belardinelli et al., 2003) at the time of the stress perturbation.

There are only few direct measures of parameter a . Laboratory experiments made by Dieterich (1980, 1981) showed that a is in the range 0.003 and 0.01. More recently, for bare granite surfaces, Kilgore et al. (1993) obtained values between 0.0103 and 0.0199, as depending on the applied normal stress. For simulated fault gouges, Mair and Marone (1999) obtained a= 0.002-0.009, as decreasing with slip at high sliding velocity (0.1-10 mm/s). This means that our reference value of a=0.003 (Table 2) is reasonable, but near the lower end of the experimentally observed range, whereas smaller values of a , suitable to increase σ_0^{max} , tend to be outside the experimental range.

In Figure 7c (open triangles), we show that using very close to failure initial condition (V_i=1 μm/s, Ψ(t=0)=1.1 L/V_i) σ_0^{max} increases up to about 10 MPa. The perturbed failure times in this case were obtained using the stress perturbations in the 26 s hypocenter with 1s rise time and the system

parameters reported in Table 2.

For 20 MPa $\leq \sigma_0 \leq$ 100 MPa and so close to failure initial conditions, the "long" term response entails failure times of the order of five minutes (250 s< t_p < 300 s, increasing with σ_0) whereas the unperturbed failure would occur at 300 s < t_u < 310 s (decreasing with σ_0). These results show that t_u-t_p< 60 s < t_u , i.e. the fault is less clock advanced than using less close to failure initial conditions, in agreement with Gomberg et al. (1998) and Belardinelli et al. (2003). Accordingly, for very close to failure initial conditions, such as those determining the open triangles in Figure 7c, we believe that the evidence of instantaneous dynamic triggering is less striking, despite the fact that indeed the fault was clock advanced or triggered even in this case. We further investigate the dependence of σ_0^{max} on the assumed initial conditions in the Appendix.

On the basis of our results, we conclude that for experimental values of the rheological parameter a , relatively small values of the initial effective normal stress at seismogenic depth the condition $\sigma_0 \leq \sigma_0^{max}$ can provide instantaneous triggering of the three early events, if a rate- and state friction law is assumed to characterize their sources. The values of initial effective normal stress suitable to reproduce instantaneous dynamic triggering can be increased up to few tens of MPa by assuming closer to failure conditions of the perturbed faults at the time of the perturbing earthquake.

5. Discussion

We show in the previous section that in order to produce a short term response of the faults to the computed stress perturbations due to the June 17, 2000 mainshock the initial effective normal stress can be increased up to a maximum value σ_0^{max} that depends on the system parameters, the stress perturbation $\Delta CFF(t)$ and the assumed initial conditions (see Appendix). In particular, σ_0^{max} increases by decreasing the rheological parameter a or considering closer to failure perturbed faults at the time of

the perturbing earthquakes. For $\sigma_0 > \sigma_0^{max}$ we have a long term or delayed effect, where the perturbed failure occurs after the end of the time varying part of the applied stress perturbation.

An original contribution of this study is the analysis of the response of a fault obeying to rate- and state-dependent friction laws to time-dependent shear and normal stress perturbations that reproduce synthetically the coseismic stress changes of a real earthquake (e.g. Figure 6). We showed that including the effect of variable normal stress in the friction law mainly affects the long term fault response in a nontrivial way (Figures 7a and 7b), that depends on the applied stress perturbations history. The most evident effect was reasonably obtained for the 8 s aftershock case, where the normal stress perturbations are not negligible with respect to the shear one.

In Figure 7 we can note a typical result of the rate- and state-dependent rheology when a non vanishing permanent part of the stress perturbation is present: the long-term or delayed response of the fault can span a large time scale, as depending continuously on initial conditions and fault system parameters (Belardinelli et al., 2003); in particular, we obtained times of perturbed failure spanning from minutes to months. By comparing the curves with open triangles with the other curves in Figure 7c, we can note that the short term effect depends scarcely on initial conditions, at least at low values of initial effective normal stress (i.e. $\sigma_0 < \sigma_0^{max}$). On the contrary, the delayed effect depends strongly on the initial conditions and the perturbed failure time t_p decreases if closer to failure initial conditions are chosen.

Concerning the short term response, our results are summarized in Table 3 for the most frequent parameter choice made in this study, including a 1.6 s rise time for the mainshock and parameter values previously specified in the text and in Table 2. From Table 3 it is evident that both the 26 s and the 30 s events followed after about two seconds the arrival time t^{II} of the second peak of Coulomb dynamic stress occurring at their hypocenters. The 8 s event followed the arrival time t^{I} of the first peak, $\Delta CFF(t^{I})$ which is about one third of $\Delta CFF(t^{II})$ at the other two hypocenters, owing to a concomitant

compressive stress phase (Figure 4). In the first column of Table 3 we also show results (in brackets) obtained for the 8 s event assuming a 25° strike and other parameters unchanged. We can note that in this case the $\Delta CFF(t^I)$ value is more than twice the value obtained with a 0° strike. In the last row we show the static CFF values resolved onto the three aftershock planes.

The values of σ_0 reported in Table 3 fulfil the condition $\sigma_0 \leq \sigma_0^{max}$ for our reference choice of parameters and initial conditions. The σ_0 values reported in Table 3 could be increased up to few tens of MPa if the used initial conditions were closer to failure (V_i>2 cm/yr and Ψ(t=0)>L/V_i), as shown in Figure 7c, or if the perturbing stress was applied close to the unperturbed failure time (Belardinelli et al., 2003). For smaller values of the initial effective normal stress than those reported in Table 3 the perturbed faults do not reach the threshold sliding velocity V_L.

In Table 3 results concerning the estimated failure times t_p of the 26 s and 30 s aftershocks show that the instantaneous dynamic triggering could be one feasible explanation for these events assuming low values of initial effective normal stress. The differences between our estimates of the failure time for these aftershocks and their origin time, however are outside the uncertainties in the aftershock origin time, but they might be reduced assuming a more complex model of fault response than the spring-slider here used. For the 8 s event we obtained similar results assuming a 25° strike, or closer to failure initial conditions for a 0° strike, the latter implying that the 8 s source fault was already going to fail at the time of the mainshock.

To complete our analysis of instantaneous dynamic triggering, we checked if low values of initial effective normal stress in the RP are compatible with the delayed triggering of the 5 minutes event that occurred near the 30 s event. In other words we investigate why this event was not instantaneously triggered, as well as the other two early events in the RP. On the basis of Arnadottir et al. (2004), in order to explain the 5 minutes event it is necessary to take into account also the 30 s event stress perturbation. For modelling the dynamic stress perturbation caused by the 30 s event we assumed the

seismic moment estimated from seismic data. Using the same parameter values assumed for the results shown in Table 3, we verified that the stress perturbations produced by both the mainshock and the 30 s event do not cause instantaneous dynamic triggering in the hypocenter of the 5 minutes event, even for $\sigma_0 < 3$ MPa. This can be explained on the basis of results shown in the Appendix, by considering that the 5 minutes event is farther from the mainshock than the other two RP events and that the 30 s earlier event did not cause dynamic ΔCFF peaks larger than 0.05 MPa in the hypocenter of the 5 minutes event. Geodetic data indicate that 30 s event could have slipped also aseismically as a slow earthquake (Arnadottir et al., 2004). Preliminary results suggest that this feature could be relevant in order to obtain a perturbed failure time of the order of minutes, for the same initial conditions assumed for the results shown in Table 3. For closer to failure initial conditions, we obtained a perturbed failure time of the order of minutes, provided that σ_0 is of the order of tens of MPa, similar to the long term effect shown by triangles in Figure 7c. A relatively high value of σ_0, could be reasonable since the shallow hypocentral depth (2.5 km) of this event might suggest hydrostatic pore pressure values. Regardless of initial conditions, the response of the fault that produced this event is delayed, and accordingly the event was certainly affected by the permanent stress perturbation caused by the 30 s event. This suggests that the 5 minute event is very likely to be a secondary aftershock of the 30 s event.

In agreement with previous studies, our results confirm that in order to have instantaneous triggering, rate- and state-dependent friction laws require the additional condition regarding a relatively low value of $\rho = \Delta CFF(t_m)/a\sigma_0$, where $t_m \leq t_p$ is the time at which the largest amplitude of ΔCFF is realized (see Appendix). For laboratory values of a, it means a relatively low value of the effective normal stress before the earthquake compared to overburden pressure. Low effective normal stress can be obtained by increasing the pore fluid pressure: if the latter approaches lithostatic pressure values, then the effective normal stress tends to vanish. Thus our results suggest a high value of pore pressure at seismogenic depth near the aftershock fault zones. Below, we argue some possible mechanisms to

provide support to the hypothesis of high pore pressure values in the fault regions where the 26 s and 30 s events occurred, related to their vicinity to the WVZ and near the Reykjanes ridge.

The events are not located in areas of known hydrothermal activity but they are close to volcanic and geothermal zones. Seismicity was already observed as remotely triggered by the passage of seismic waves of the 1992 Landers earthquake, the 1999 Hector Mine earthquake and the 2002 Denali earthquake in the geothermal area of Long Valley (e.g. Brodsky and Prejan, 2005) and in the Yellowstone caldera after the Denali earthquake (Eberhart-Phillips et al., 2003, Husen et al., 2004). Both the Hengill region (Figure 1) and the Krisuvìk region, west of Lake Kleifarvatn (close to the 30 s epicenter in Figure 1) are geothermal areas (e.g. see Rognvaldsson et al., 1998, Clifton et al., 2003). The 26 s event is located near the SW edge of the Brennisteinsfjöll volcanic system (Pagli et al., 2003). Fournier (1991) provides evidences of greater than hydrostatic pore pressure values in regions characterized by temperatures exceeding 370 °C where rocks may behave as plastic with low permeabilities values (Hill et al., 1993); in particular, he presents the case of fluids entering the bottom of a geothermal exploration well at Nesjavellir, in the upper NE flank of the Hengill volcano (about 2200 m depth). Permeability may also decrease due to solubility reduction and precipitation of minerals clogging fractures (Fournier, 1991).

We point out that in the geothermal areas where hydrothermal activity is observed, fluid circulation reaches the surface and pore pressure values are expected to be nearly hydrostatic. Therefore geothermal regions characterized by high geothermal gradients may have high pore pressure fluids at depth even if no hydrothermal activity is observed at the surface, as it happens in the regions where the epicenters of the early events are located.

In general, to explain high values of pore pressure in fault zones, one can consider that fluids provided by a source near the ductile roots of faults should be characterized by pore pressure approaching the lithostatic values (Rice, 1992), thus providing very small effective normal stress. GPS

data collected in the RP between 1986 and 2001 suggest that left-lateral shear ductile deformation occurs in this area below a locking depth of about 6 km (Hreinsdottir et al., 2001, Clifton et al., 2003, Pagli et al., 2003). Owing also to the vicinity to the Reykjanes Ridge, the basis of the relatively young brittle crust (the depth above which 90% of well located events occurs in the period 1990-1999) in the 26 s and 30 s aftershock region is estimated as 6-7 km (Tryggvason et al., 2002). Therefore the ductile roots of the source faults of these two aftershocks can be estimated at relatively shallow depth, supporting the hypothesis of small initial effective normal stress values at the location of the two aftershocks.

6. Conclusive Remarks

In this paper we had the rare opportunity to consider evidences of early aftershocks both in near field and in far field conditions. We analyzed three of the major early aftershocks occurring in the first minutes after the mainshock in the South Iceland Seismic Zone in terms of dynamic stress interaction or triggering.

The study of the dynamic stress variation generated by the June 17, 2000 mainshock in the SISZ allowed us to estimate the arrival time and the amplitude of $\Delta CFF(t)$ peaks at the hypocenters of three early events occurring in the first minute after the mainshock in the SISZ and along its prolongation in RP (Figure 1). Furthermore a one-dimensional fault model based on rate- and state-dependent friction laws provided us the estimated failure time t_p of a fault perturbed by the dynamic shear stress and normal stress computed at the three hypocenters. The tree early events can be reproduced as triggered dynamically, that is we estimated failure times that correlate with the measured origin times.

Our study suggests that, except for very close to failure initial conditions of the fault (such that the triggering effect in principle might be less striking) in order to have instantaneous triggering, rate- and state-dependent friction laws require the additional condition regarding a relatively low value of the

initial effective normal stress compared to overburden pressure, i. e. high pore pressure values. Laboratory studies of the frictional behaviour of sliding surfaces with smectite gouges interposed support the idea that faults can host earthquake-like unstable ruptures ($b - a > 0$ in equation 2) at seismogenic depth, even in the presence of low effective normal stress (Saffer et al., 2001). High values of pore fluid pressure are suggested by polarization of shear wave splitting data recorded in the seismically active area of Husavik-Flatey Fault in North of Iceland (Crampin et al., 2002).

Acknowledgements

The autorhs wish to thank two anonymous referees and Richard Archulus that greatly improved the original version of the manuscript. We also thank Ragnar Stefansson, Massimo Cocco, Joan Gomberg, Sandy Steacy and Maurizio Bonafede for fruitful comments and discussions. This research was supported by the funds of the European Community, under contract EVG1-CT-2002-00073 (project "PREPARED").

Appendix.

In Figure 7 we show that σ_0^{max}, the maximum value of the initial effective normal stress to obtain the short term response, is different for each stress perturbation considered. In this Appendix we further investigate the condition $\sigma_0 \leq \sigma_0^{max}$ and show that it is related to a more general condition to obtain a short term response of the perturbed fault.

We performed several numerical simulations with varying the rheological parameter a, the initial effective normal stress σ_0 and the perturbing stress at the hypocenters of the three events within its uncertainties. We will refer this set of tests as "global". We performed two global sets of tests for two values of initial velocity V_i. Our simulations generally show that instantaneous triggering tends to occur

soon after t_m, the first instant of time since the mainshock when $\Delta CFF(t)$ is such that $\Delta CFF(t_m)/(a\sigma_0) \equiv \rho \geq \rho_{min}$. The threshold ratio $\rho_{\min}$ is approximately constant in each global set of tests and depends on the initial conditions of the system, as will be shown below. Therefore on the basis of our tests the general condition to have a short term response can be expressed as $\rho \geq \rho_{\min}$. If $\Delta CFF(t) < \rho_{\min} a\sigma_0, \forall t$, the perturbed failure tends to occur after the end of the time varying stress perturbation (i.e. when $\Delta\tau(t_p) = \Delta\sigma(t_p) = 0$).

For $\sigma_n^{eff} = \sigma_0 (\Delta\sigma = 0)$ and a assigned, as in Belardinelli et al. (2003), the condition $\rho \geq \rho_{\min}$ entails a threshold $\Delta\tau_c \equiv \rho_{\min} a\sigma_0$ for the amplitude perturbing shear stress. For $\Delta\tau$(t) and a assigned, as in the present study, the condition $\rho \geq \rho_{\min}$ translates into $\sigma_0 \leq \sigma_0^{\max}$, where $\sigma_0^{\max} = \Delta\tau(t)/(a\rho_{\min})$. Therefore the existence of a maximum value of the initial effective normal stress $\sigma_0^{\max}$ to obtain a short term response (Figure 7) is a consequence of the existence of a ratio threshold value ρ_{min}. At the same time, the condition $\rho \geq \rho_{\min}$ was already verified in previous studies that were starting from a different point of view than currently assumed. In agreement with our global sets of tests, in Figure 7 it is clear that the maximum value of initial effective normal stress, $\sigma_0^{\max}$ depends on $\Delta CFF(t)$.

To favor the short term response without changing the value of σ_0 it is sufficient to increase the $\sigma_0^{\max}$ value. From its definition, $\sigma_0^{\max}$ can be increased either decreasing a or ρ_{min}. The threshold ratio ρ_{min} can be decreased by assuming a higher initial velocity or "a closer to failure" perturbed fault at the time of the mainshock, as we verified in agreement with results obtained by Perfettini et al. (2003) with square wave of shear stress applied to a spring-slider model. In the first global set of tests we assume V_i=2 cm/yr and $\Psi(t=0)=L/V_i$ as in most of the simulations shown in the present study, obtaining $\rho_{\min} \cong 14$. A smaller value ($\rho_{\min} \cong 11$) can be obtained if the initial velocity is increased by one order

of magnitude, i.e. V_i=20 cm/yr , as we found in the second global set of tests. In particular in Figure 7c, using even closer to failure initial condition (V_i=1μ m/s, $\Psi(t=0)$=1.1L/V_i) and the stress perturbations in the 26 s hypocenter obtained with a 1s rise time and other parameters unchanged (Table 2), $\sigma_0^{\max}$ increases up to about 10 MPa and $\rho_{\min} \cong 5$, since $\Delta CFF(t)$ = 0.158 MPa (with $t_m=t^{II}$).

References

Antonioli, M., M. Cocco, S. Das, and C. Henry (2003), Dynamic stress triggering during the great 25 March 1998 Antarctic Plate earthquake, *Bull. Seismol. Soc. Am.*, *92*(3), 896-903.

Antonioli, A., M.E. Belardinelli, and M. Cocco (2004), Modelling dynamic stress changes caused by an extended rupture in an elastic stratified half space, Geophys. J. Int., 157, 229-244, doi:10.1111/j.1365-246X.2004.02170.x.

Arnadottir, T., S. Jonsson, R. Pedersen, and G. B. Gudmundsson (2003), Coulomb stress changes in the South Iceland Seismic Zone due to two large earthquakes in June 2000, Geophys. Res. Lett., 30 (5), doi:10.1029/2002GL016495.

Arnadottir, T. (2004), WP 2.3 Long-term deformation in the South Iceland Seismic Zone (SISZ) inferred by joint interpretation of GPS, INSAR and borehole strain data, in the First Periodic Report of EEC Contract no. EVG1-CT-2002-00073,"PREPARED", section 3, pp. 21-26.

Arnadottir, T., H. Geirsson and P. Einarsson (2004), Coseismic stress changes and crustal deformation on the Reykjanes Peninsula due to triggered earthquakes on 17 June 2000, J. Geophys. Res., 109, doi:10.1029/2004JB003130

Arnadottir, T., Jiang W., Feigl K. L., Geirsson H. and E. Sturkell (2005), The crustal deformation field of southwest Iceland derived from GPS surveys: 1992 through 2004, Geophysical Research Abstracts, Vol. 7, 09859.

Belardinelli, M. E., M. Cocco, O. Coutant, and F. Cotton (1999), Redistribution of dynamic stress

during coseismic ruptures: Evidence for fault interaction and earthquake triggering, *J. Geophys. Res.*, 104(B7), 14,925– 14,946.

Belardinelli, M. E., M. Bonafede and A. Gudmundsson (2000), Secondary earthquake fracture generated by a strike-slip fault in the South Iceland Seismic Zone, *J. Geophys. Res.,* 105 (B6), 13613 13629.

Belardinelli, M.E., A. Bizzarri, and M. Cocco (2003), Earthquake triggering by static and dynamic stress changes, *J. Geophys. Res.*, *108*(B3), 2135, doi: 10.1029/2002JB001779.

Boatwright, J., and M. Cocco (1996), Frictional constraints on crustal faulting, *J. Geophys. Res.*, 101, 13895-13910.

Brodsky, E., V. Karakostas, and H. Kanamori (2000), A new observation of dynamically triggered regional seismicity: Earthquakes in Greece following the August, 1999 Izmit, Turkey earthquake, *Geophys*. *Res*. *Lett*., 27(7), 2741-2744.

Brodsky, E. E., and S. G. Prejean (2005), New constraints on mechanisms of remotely triggered seismicity at Long Valley Caldera, *J. Geophys. Res.*, *110*, B04302, doi:10.1029/2004JB003211.

Clifton, A.E., C. Pagli, J.F. Jonsdottir, K. Eythorsdottir, and K. Vogfjord (2003), Surface effects of triggered fault slip on Reykjanes Peninsula, SW Iceland, *Tectonophysics*, 369(3-4), 145-154.

Clifton, A.E. and P. Einarsson (2005), Styles of surface rupture accompanying the June 17 and 21, 2000 earthquakes in the South Iceland Seismic Zone, *Tectonophysics*, 396, (3-4), 141- 159.

Clifton, A.E. ,M. J. Roberts M. J., Guðmundsson G.B., Halldórsson P. and P. Einarsson (2005), Spatial and temporal distribution of earthquakes on the Reykjanes Peninsula: their relationship to faults and implications for hazard assessment, *Geophysical Research Abstracts*, Vol. 7, 03370.

Cotton, F., and O. Coutant (1997), Dynamic stress variations due to shear faults in a plane layered medium, *Geophys. J. Int.*, 128, 676-688.

Crampin, S., Volti, T, Chastin, S., Gudmundsson, A. and R. Stefansson (2002), Indication of high pore

fluid pressures in a seismically-active fault zone, *Geophys. J. Int.,* 151, F1–F5.

Dieterich J. H. (1980), Experimental and model study of fault constitutive properties, *Solid Earth Geophysics and Geotecnology, Appl. Mech. Div.*, 42, edited by S. Nemat-Nasser, *American Society of Mechanical Engineers*, New York, pp.103-120, 21-29.

Dieterich J. H. (1981), Constitutive properties of faults with simulated gouge, *Mechanical Behavior of Crustal Rocks, Geophysical Monograph*, 24, edited by N. L. Carter, M. Friedman, J. M. Logan and D. W. Stearns, *Am. Geophys. Union*, Washington D. C., pp. 103-12.

Dieterich J., H., and M., F. Linker (1992), Fault stability under conditions of variable normal stress, *Geophys. Res. Lett*, 19 (16), 1691-1694.

Eberhart-Phillips, D. et al. (2003), The 2002 Denali Fault Earthquake, Alaska: A large magnitude, slip partitioned event. *Science* 300(5622), 1113–1118.

Einarsson, P., S. Bjornsson, G. Foulger, R. Stefansson, and Th. Skaftadottir (1981), Seismicity pattern in the South Iceland Seismic Zone, in *Earthquake Prediction – An international review*, edited by

D. W. Simpson and P. G. Richards, EOS Transaction, vol. 4, 141–151.

Felzer, K. R., T. W. Becker, R. E. Abercrombie, G. Ekström, and J. R. Rice (2002), Triggering of the 1999 *Mw* 7.1 Hector Mine earthquake by aftershocks of the 1992 *Mw* 7.3 Landers earthquake, *J. Geophys. Res.*, *107*(B9), 2190, doi:10.1029/2001JB000911.

Fournier, R. O. (1991), The transition from hydrostatic to greater than hydrostatic fluid pressure in presently active continental hydrothermal systems in crystalline rock, *Geophys*. *Res*. *Lett*., 18(5), 955 958.

Gomberg, J., M. L. Blanpied, and N. M. Beeler (1997), Transient triggering of near and distant earthquakes, *Bull. Seismol. Soc. Am.*, 87(2), 294 –309.

Gomberg, J., N. M. Beeler, M. L. Blanpied, and P. Bodin (1998), Earthquake triggering by transient and static deformations, *J. Geophys. Res.*, 103(10), 24,411 –24,426.

Gomberg, J., P. Bodin, K. Larson, and H. Dragert (2004), Earthquake nucleation by transient deformations caused by the M = 7.9 Denali, Alaska, earthquake, *Nature*, 427, 621-624.

Gomberg, J., P. A. Reasenberg, M. Cocco, and M.E. Belardinelli (2005), A frictional population model of seismicity rate change, *J. Geophys. Res*., 110, B05S03, doi:10.1029/2004JB003404

Harris, R. A., and S. M. Day (1993), Dynamics of fault interaction: parallel strike slip faults, *J. Geophys. Res*., 98(3), 4461-4472.

Harris, R. A., (1998), Introduction to special section: Stress triggers, stress shadows, and implications for seismic hazard, *J. Geophys. Res.*, 103(B10), 24347-24358.

Hill, D. P. et al. (1993), Seismicity remotely triggered by magnitude 7.3 Landers, California, earthquake, *Science*, 260, 1617-1623.

Hjaltadottir S., Vogfjord K. S. and R. Slunga (2005) mapping subsurface faults in southwest Iceland using relatively located micro earthquakes, *Geophysical Research Abstracts*, Vol. 7, 06664.

Hreinsdottir, S., P. Einarsson, and F. Sigmundsson (2001). Crustal deformation at the oblique spreading Reykjanes Peninsula, SW Iceland: GPS measurements from 1993 to 1998, *J. Geophys. Res.*, 106, 13803-13816.

Husen S, Taylor R, Smith RB, et al. (2004), Changes in geyser eruption behavior and remotely triggered seismicity in Yellowstone National Park produced by the 2002 M 7.9 Denali fault earthquake, Alaska, *Geology* 32 (6): 537-540.

Kilb, D., J. Gomberg, and P. Bodin (2000), Earthquake triggering by dynamic stresses, *Nature*, 408(6821), 570-574.

Kilgore B.D., Blanpied, M.L. and J.H. Dieterich (1993), Velocity dependent friction of granite over a wide range of conditions, *Geophys. Res. Lett*., 20(10), 903-906.

Jònsson, S., P. Segall, R. Pedersen, and G. Bjornsson (2003), Post-earthquake ground movements correlated to pore-pressure transients, *Nature*, 424(6945), 179-183.

Linker, M. F., and J H. Dieterich (1992), Effects of variable normal stress on rock friction: observations and constitutive equations, *J Geophys. Res.*, 97(4), 4932-4940.

Mair , K., and C. Marone (1999), Friction of simulated fault gouge for a wide range of velocities and normal stresses, *J. Geophys. Res.*, 104(12), 28899-28914.

Monelli, D. (2004), Interazione tra faglie sismiche in un modello dinamico 3D, Degree Thesis n. 2928, a.a. 2003-2004, Library of the Physics Department, University of Bologna.

Pagli, C., R. Pedersen, F. Sigmundsson and K.L. Feigl (2003). Triggered fault slip on June 17, 2000 on the Reykjanes Peninsula, SW-Iceland captured by radar interferometry, *Geophys. Res. Lett*., 30 (6), 1273, doi:10.1029/2002GL015310.

Parson, T. (2005), A hypothesis for delayed dynamic earthquake triggering, *Geophys. Res. Lett*., 32, L04302, doi:10.1029/2004GL021811.

Pedersen, R., F Sigmundsson, K. L. Feigl and T. Arnadottir (2001), Coseismic interferograms of two Ms=6.6 earthquakes in the South Iceland Seismic Zone, June 2000, *Geophys. Res. Lett.*, 28 (17), 3341-3344.

Pedersen, R., S. Jonsson, T. Arnadottir, F. Sigmundsson, and K.L. Feigl (2003), Fault slip distribution of two June 2000 Mw 6.5 earthquakes in South Iceland estimated from joint inversion of InSAR and GPS measurements, *Earth Planet. Sci Lett,* 213(3-4), 487-502.

Perfettini, H., J. Schmittbuhl, and A. Cochard (2003), Shear and normal load perturbations on a two-dimensional continuous fault: 2. Dynamic triggering, *J. Geophys. Res.*, *108*(B9), 2409, doi: 10.1029/2002JB001805.

Rice, J. (1992), Fault stress states, pore pressure distributions, and the weakness of the San Andreas fault. Fault mechanics and transport properties of rocks. *A Festschrift in Honor of W. F. Brace* (based on June 1990 symposium at MIT), edited by Brian Evans and Teng-Fong Wong, Academic Press, London, 475-503.

Roy, M. and C. Marone (1996), Earthquake nucleation on model faults with rate- and state-dependent friction: Effects of inertia, *J. Geophys. Res.*, *101*(B6), 13919-13932.

Rognvaldsson, S. T., G. B. Gudmundsson, K. Agustsson, S. S. Jakobsdottir, R. Slunga, and R. Stefansson (1998), Overview of the 1993-1996 seismicity near Hengill, *VI R98006-JAO5*, Icelandic Meteorological Office.

Saffer, D.M., K.M. Frye, C. Marone and K. Mair (2001), Laboratory results indicating complex and potentially unstable frictional behavior of smectite clay, *Geophys. Res. Lett.*, 28 (12), 2297-2300.

Stefansson, R., G. Gudmundsson and P. Haldòrsson (2003), The South Iceland earthquakes 2000 a challenge for earthquake prediction research, URL: http://hraun.vedur.is/ja/prepared/SouthIcelandEarthq2000/, last modified April 2 2003.

Tibi, R., Wiens, D.A., and H. Inoue (2003), Remote triggering of deep earthquakes in the 2002 Tonga sequences, *Nature*, *424*, 921-925.

Tinti, E., A., Bizzarri, A. Piatanesi, and M. Cocco (2004). Estimates of slip weakening distance for different dynamic rupture models, *Geophys. Res. Lett.,* 31, L02611, doi:10.1029/2003GL018811.

Tryggvason A., S. Th. Rognvaldsson and O. G. Flovenz (2002), Three-dimensional imaging of the P and S-wave velocity structure and earthquake locations beneath Southwest Iceland, *Geophys. J. Int*., *151*(3), 848-866.

Vogfjord, K.S., G. Nolet, W.J. Morgan, R. Allen, R. Slunga, B. Bergsson, P. Erlendsson, G. Foulger, S. Jakobsdottir, B. Julian, M. Pritchard, S. Ragnarsson, and R. Stefansson (2002), Crustal profiling in Iceland using earthquake source arrays, *EOS. Trans. AGU*, *83*(45), Fall Meet. Suppl. Abstract S61C 1161.

Vogfjord, K. (2003), Triggered seismicity after the June 17, M_w=6.5 earthquake in the South Iceland Seismic Zone: the first five minutes, *Geophys. Res. Abstracts, 5*, 11251.

Vogfjord, K.S, S. Hjaltadottir, and R. Slunga (2005). The M≈5 triggered events in the South Iceland

Seismic Zone of June 17, 2000: Determination of fault plane, magnitude and mechanism, *Geophysical Res. Abstracts*, vol.7, 10274.

Voisin, C., M. Campillo, I. Ionescu, F. Cotton, and O. Scotti (2000), Dynamic versus static stress triggering and friction parameters: Inferences from the November 23, 1980, Irpinia earthquake, *J. Geophys. Res*., *105*(9), 21,647-21,659.

Voisin, C., F. Cotton, and S. Di Carli (2004), A unified model for dynamic and static stress triggering of aftershocks, antishocks, remote seismicity, creep events, and multi segmented rupture, *J. Geophys. Res.*, *109*, B06304, doi:10.1029/2003JB002886.

Weir, N. R. W., R. S. White, B. Bransdottir, P. Einarsson, H. Shimamura, and H. Shiobara (2001), Crustal structure of the northern Reykjanes Ridge and Reykjanes Peninsula, southwest Iceland, *J. Geophys. Res.*, *106*(B4), 6347-6368.

Ziv, A. (2003), Foreshocks, aftershocks, and remote triggering in quasi-static fault models, *J. Geophys. Res.*, *108*(B10,) 2498, doi:10.1029/2002JB002318.

Figure 1. Map of the studied area: the South Iceland Seismic Zone (SISZ) and the Reykjanes Peninsula (RP). The epicenter locations of the two largest events of the June 2000 sequence (June 17 and June 21) are shown by the dark stars and the three largest aftershocks occurring in the first minute after the June 17 mainshock are shown by white stars, with their origin times (s) relative to the mainshock. The shaded area delimitates the map shown in Figure 3. The inset map of Iceland shows the study area. "He" marks the location of Hengill volcano. WVZ and EVZ denote the Western Volcanic Zone and the Eastern Volcanic Zone, respectively.

Figure 2. Velocity profiles with four layers adopted in the simulations (solid lines). The four layer profiles refer to the structure East of Hengill ("He" in Figure 1, from Vogfjord et al., 2002). The dotted lines, reported for comparison, refer to a gradient model suitable for the region West of Hengill (see also Weir et al., 2001). We assume density values of 2300 kg/m^3 from 0 to 1100 m, 2540 kg/m^3 from 1100 to 3100 m, 3050 kg/m^3 from 3100 to 7800 m and 3200 kg/m^3 at depths larger than 7800 m.

Figure 3. Maps of the *CFF* variations on the RP region shown in Figure 1. The yellow dots are the epicentral locations of the two $M_l > 5$ dynamically triggered aftershocks (at 26 s and 30 s after the mainshock). The maps are computed at a depth of 8.9 km. The black solid curve is the coastal line of the RP. Snap shots are shown for 22, 26, 30 and 34 seconds.

Figure 4. ΔCFF , $\Delta\tau$ and $\Delta\sigma$ time evolution at the hypocentral location of the 8 s earthquake. Values of computed stress changes at the observed origin time of the earthquake are marked by symbols (open circle for $\Delta\tau$, open diamond for $\Delta\sigma$ and filled circle for ΔCFF). The time occurrences of the

first two peaks of dynamic ΔCFF are also indicated by t^I and t^{II}. A 1.6 s rise time is used.

Figure 5. Same as Figure 4 for the two events occurred at 26 (a) and 30 (b) seconds after the mainshock. ΔCFF, $\Delta\tau$ and $\Delta\sigma$ time evolution is evaluated at the hypocentral locations of the two events. A 1.6 s rise time is used.

Figure 6. Dynamic instantaneous response of a spring-slider system to the stress perturbation $\Delta\tau(t)$ and $\Delta\sigma(t)$ obtained in the 26 s aftershock hypocenter with a 1.6 s rise time. In panel (a) we represent the evolution of the total loading traction, in panel (b) the total effective normal stress. In panel (c) the sliding velocity is shown as a function of time with indication of the failure instant of time t_p when the sliding velocity exceeds V_L= 10 cm/s. In panel (d) the state variable evolution is represented. We assumed parameters values as in Table 2 and in the text, with α_{DL}=0.3 and σ_0=2.5 MPa. The ~ 1.4 s delay of the fault response with respect to the time of the second peak of applied shear stress is indicated.

Figure 7. Failure time t_p as a function of the initial effective normal stress σ_0 obtained with applying the stress history $\Delta\tau(t)$ and $\Delta\sigma(t)$ computed in the 8 s hypocenter (panel (a)) and in the 26 s aftershock hypocenter with a 1.6 s rise time (panel (b)), for three values of the α_{DL} parameter. A 1.6 s rise time is used. In panel (c) we consider α_{DL}=0.3 and different stress perturbations $\Delta\tau(t)$ and $\Delta\sigma(t)$ evaluated at the 26 s hypocenter with varying the rise time. At low values of σ_0, circles (2 s rise time) are missing in panel (c), since the fault does not reach the threshold slip velocity in these cases ($V(t)<V_L, \ \forall t$). Parameter values are those reported in Table 2 and in the text, in particular V_i = 2 cm/yr and $\Psi(0)=L/V_i$, except for open triangles in panel (c) where we used closer to failure initial conditions

($V_i = 1\mu$ m/s and $\Psi(t=0) = 1.1\ L/V_i$). A short term response of the fault ($t_p \approx$ tens of seconds) is evident only for low values of initial effective normal stress ($\sigma_0 \leq 3.5$ MPa). In these cases t_p tends to follow a peak of the applied shear stress perturbation, $\Delta\tau(t)$, by 2 s or less.

Table 1. Aftershock parameters.

Origin time	Latitude (°)	Longitude (°)	Depth (km)	M_l
15:40:49	**64.020**	**-20.86**	**9.0**	**~ 3.5**
15:41:07	**63.951**	**-21.69**	**8.9**	**~ 5.5**
15:41:11	**63.937**	**-21.94**	**3.8**	**~ 5.5**

Table 2. Fault failure parameters.

μ_*	**0.7**
a	**$3\ 10^{-3}$**
b	**10^{-2}**
L (μm)	**10^3**
α_{DL}	**0.3**
m (kg/m2)	**$1.9\ 10^6$**
k (MPa/⌈m)	**$3\ 10^{-6}$**
V_i (cm/yr)	**2***
V_o (cm/yr) **2**	**2**
V_L (m/s)	**0.1**

* In the preseismic period 1992-1999, geodetic data (Arnadottir, 2004, Arnadottir et al., 2005) show that the SISZ and in particular the RP were subjected to shear strain rate values > 0.2 μ strain/yr that are indicative of left lateral motion on a E-W transform zone or right lateral motion on N-S faults. Assuming the strain rate to be accommodated on a region of about 100 km EW width, we obtain for V_i a value at least equal to 2 cm/yr, the observed spreading rate in the SISZ.

Table 3. Summary of results for spring-slider parameters listed in Table 2, in the case of $\Psi(t=0) = L/V_i$, and α_{DL}=0.3 a 1.6 s rise time for the mainshock.

Origin time (s)	**7.8+/-0.1***	**25.9+/-0.1**	**30.3 +/-0.2**
t^I **(s)**	5.39 (5.86)	14.06	15.94
$\Delta CFF(t^I)$ **(MPa)**	0.043 (0.105)	0.037	0.021
t^{II} **(s)**	12.2 (12.4)	24.14	27.89
$\Delta CFF(t^{II})$ **(MPa)**	0.132 (0.192)	0.111	0.129
t_p **(s)**	12.5-13.5 (6.3-7.9)	24.6-25.5	28.0-29.1
σ_0 **(MPa)**	1.5-3.0 (1.5-2.5)	1.5-2.5	1.5-3.0
ΔCFF_{stat} **(MPa)**	0.025 (0.054)	0.006	0.003

*The values shown between brackets in this column are obtained assuming a 8 s fault orientation with 25° strike, 90° dip, 180° rake.

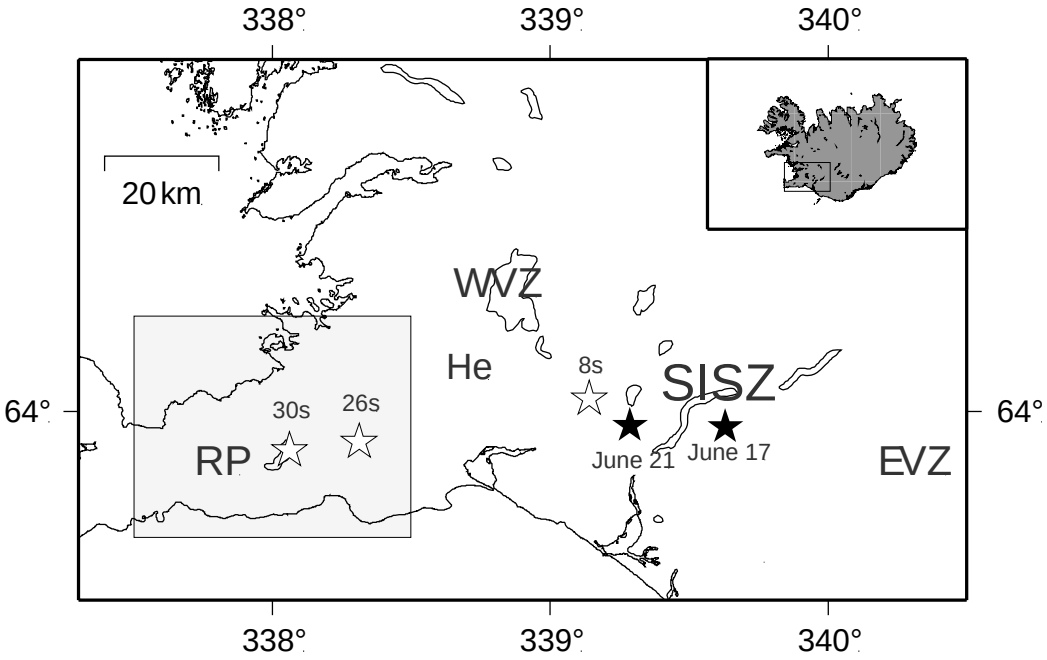
338°
339°
340°
20 km
WVZ
He
8s
SISZ
64°
30s
26s
RP
June 21
June 17
EVZ
64°
338°
339°
340°

Figure 1

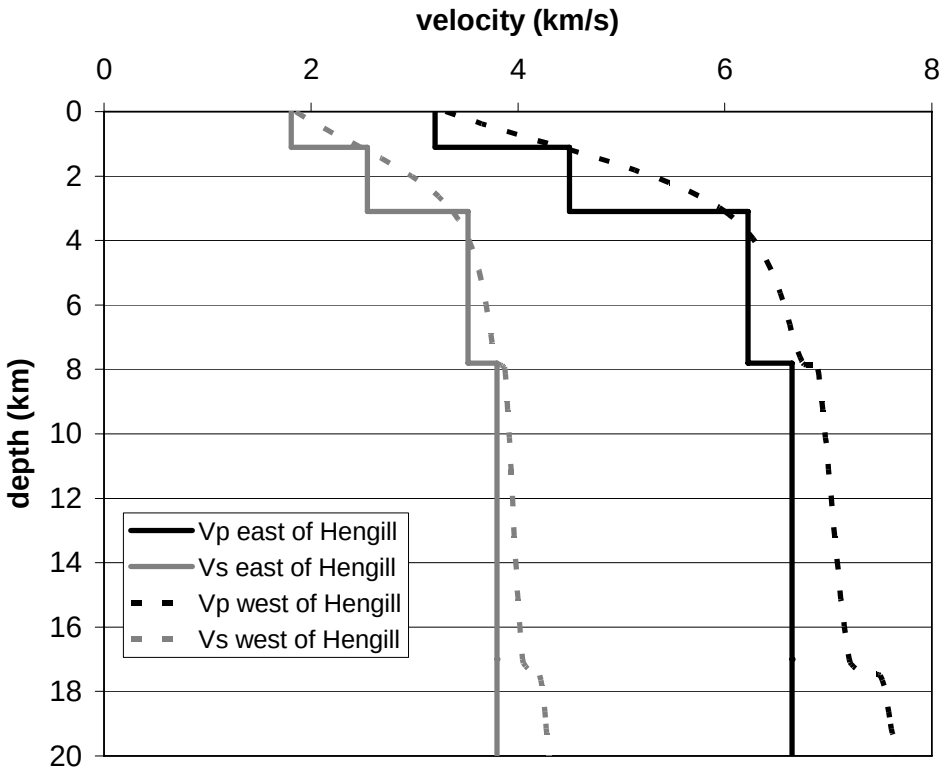
velocity (km/s)
0
2
4
6
8
depth (km)
0
2
4
6
8
10
12
14
16
18
20
Vp east of Hengill
Vs east of Hengill
Vp west of Hengill
Vs west of Hengill

Figure 2

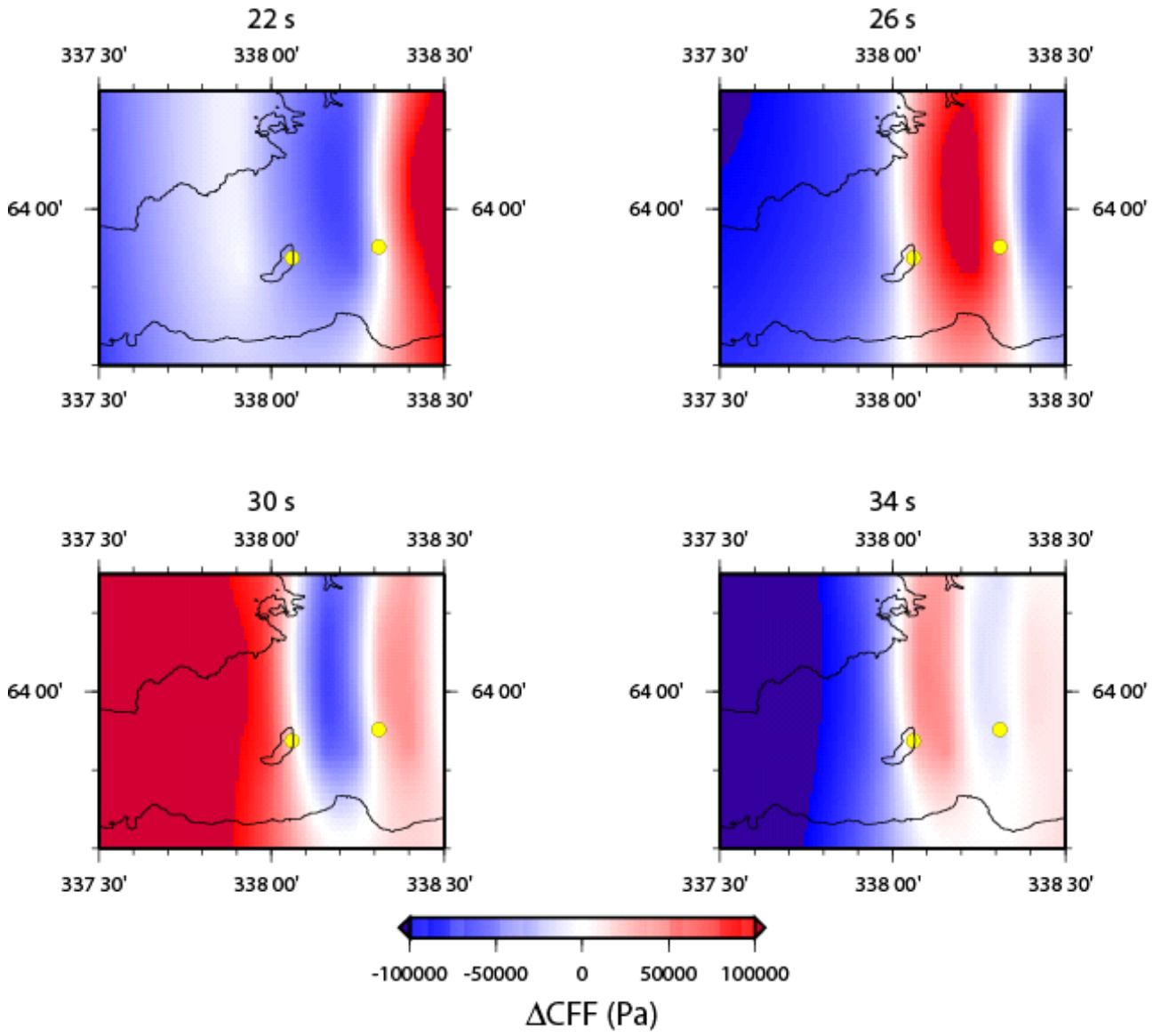
b
22 s
26 s
30 s
34 s
337 30'
338 00'
338 30'
64 00'
-100000
-50000
0
50000
100000
ΔCFF (Pa)

Figure 3

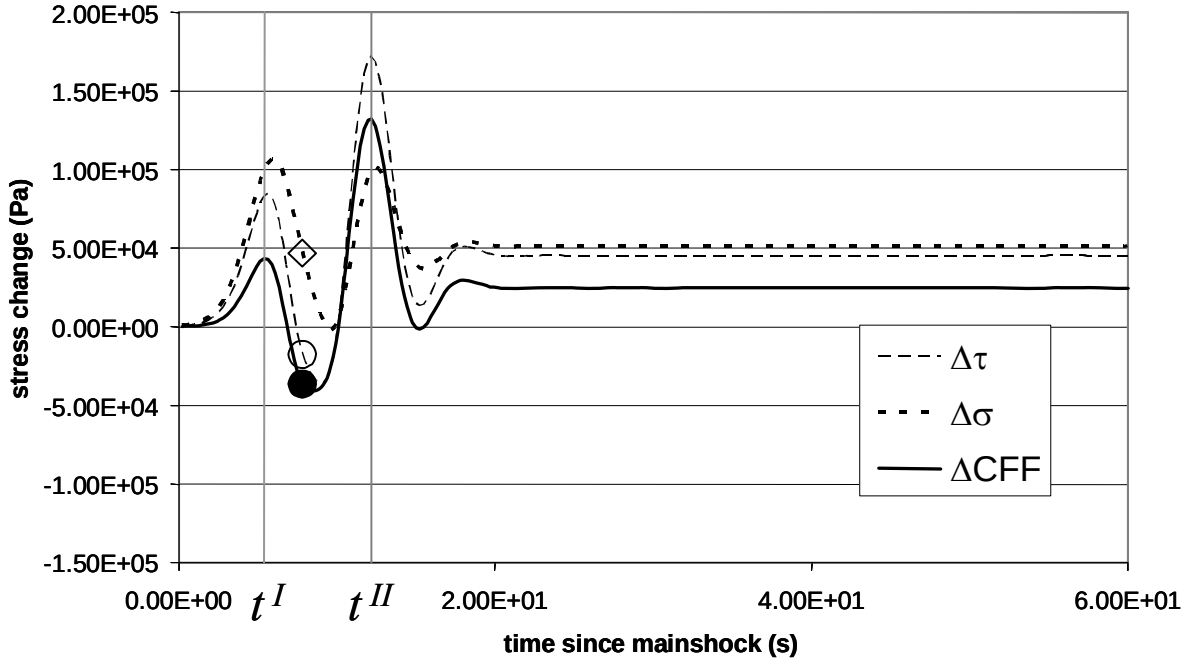
2.00E+05
1.50E+05
1.00E+05
5.00E+04
0.00E+00
-5.00E+04
-1.00E+05
-1.50E+05
stress change (Pa)
0.00E+00
t^I
t^{II}
2.00E+01
4.00E+01
6.00E+01
time since mainshock (s)
Δτ
Δσ
ΔCFF

Figure 4

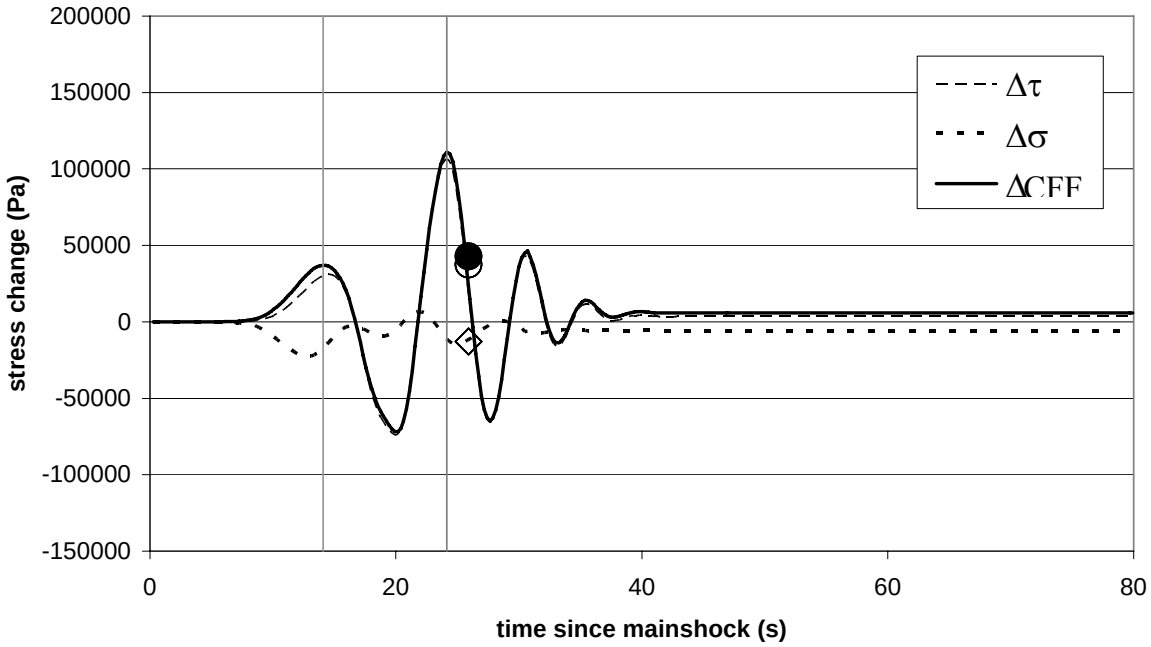
200000
150000
100000
50000
0
-50000
-100000
-150000
stress change (Pa)
0
20
40
60
80
time since mainshock (s)
Δτ
Δσ
ΔCFF

(a)

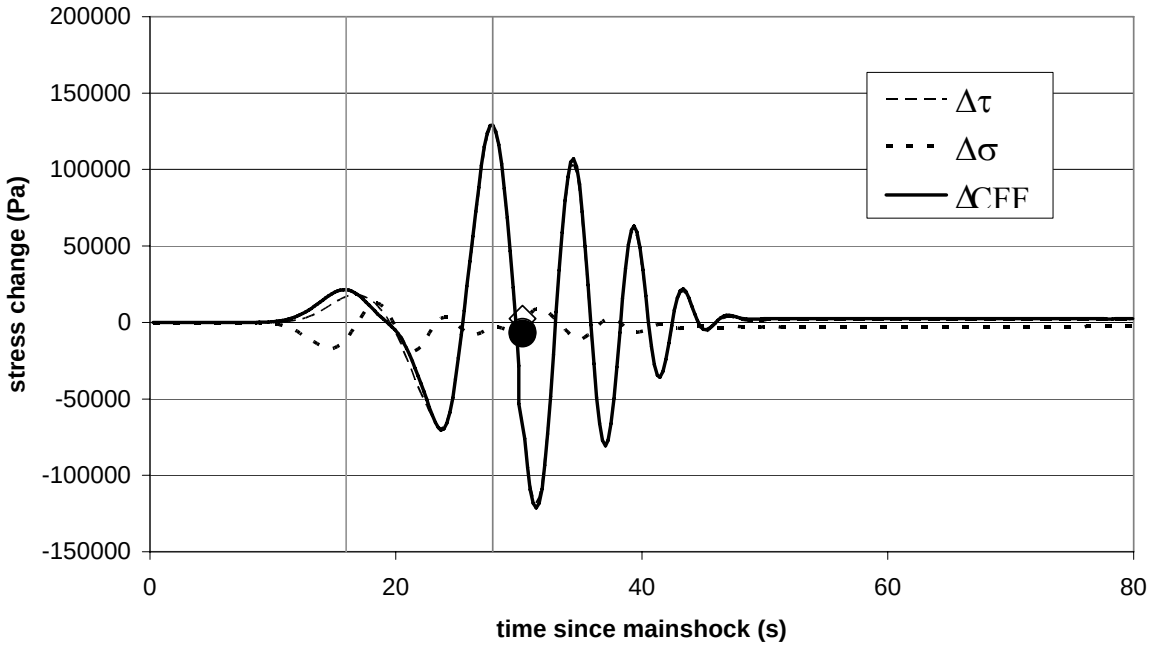
200000
150000
100000
50000
0
-50000
-100000
-150000
stress change (Pa)
0
20
40
60
80
time since mainshock (s)
Δτ
Δσ
ΔCFF

(b)

Figure 5

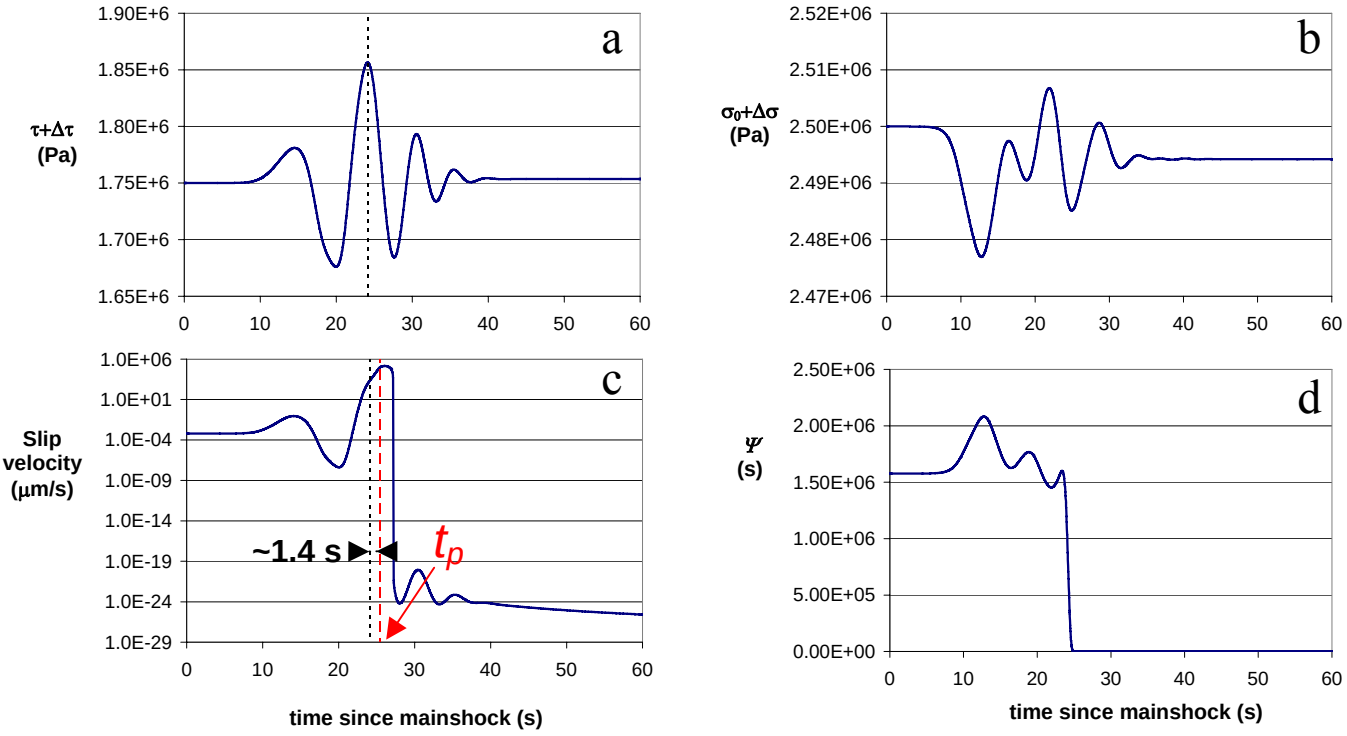
a
b
c
d
τ+Δτ (Pa)
σ0+Δσ (Pa)
Slip velocity (μm/s)
Ψ (s)
~1.4 s
tp
time since mainshock (s)
time since mainshock (s)

Figure 6

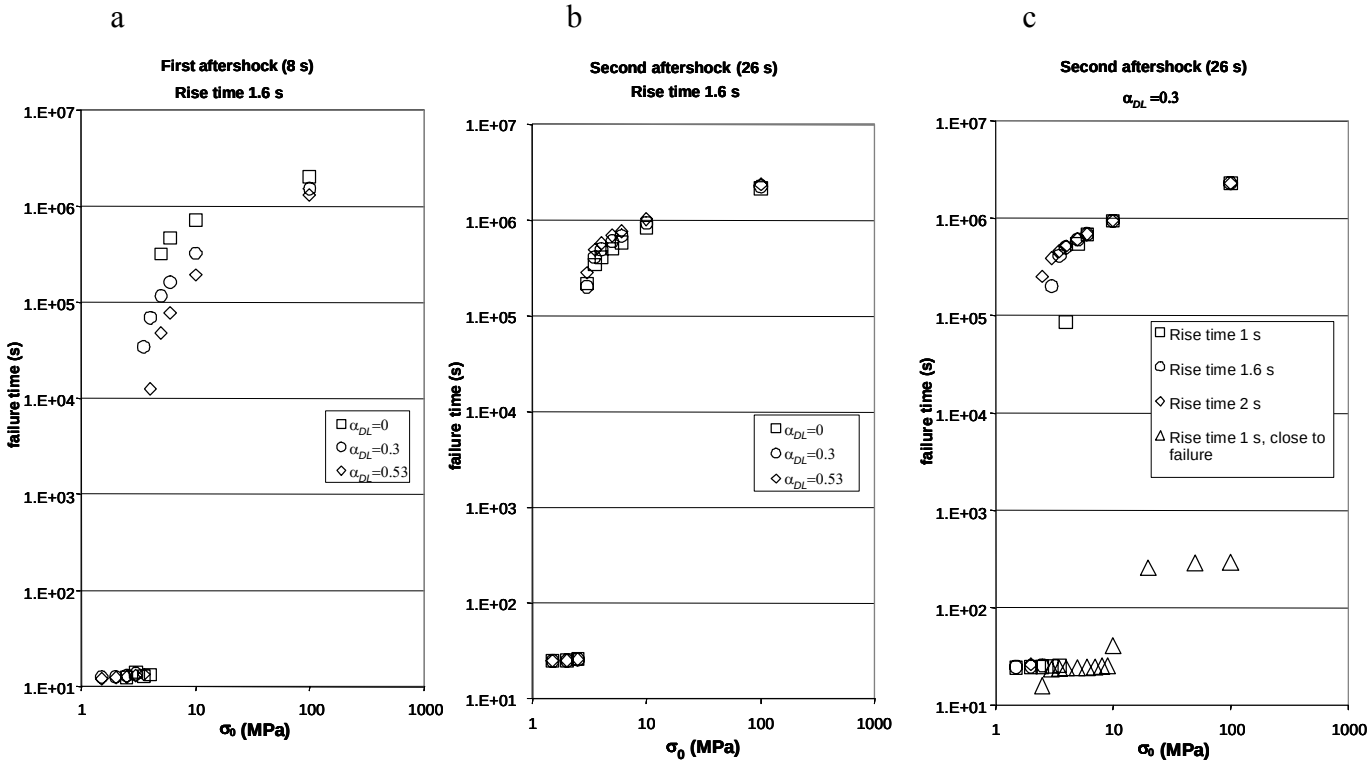
a
b
c
First aftershock (8 s)
Rise time 1.6 s
Second aftershock (26 s)
Rise time 1.6 s
Second aftershock (26 s)
α_{DL} =0.3
failure time (s)
1.E+07
1.E+06
1.E+05
1.E+04
1.E+03
1.E+02
1.E+01
1
10
100
1000
σ_0 (MPa)
α_{DL}=0
α_{DL}=0.3
α_{DL}=0.53
Rise time 1 s
Rise time 1.6 s
Rise time 2 s
Rise time 1 s, close to failure

Figure 7